arXiv:physics/0411210v2 [physics.chem-ph] 8 Dec 2004

Three Different Sizes Obtained Using Light Scattering Techniques

Yong Sun

February 2, 2008

Abstract

The average scattered intensity is determined by the optical characteristics of particles in dispersion. The normalized time auto-correlation function of the scattered light intensity $g^{(2)}(\tau)$ includes both the optical and hydrodynamic information of particles. From the different characteristics of particles, the particle sizes can be obtained. In this paper, three sizes: the static radius R_s, the hydrodynamic radius R_h and the apparent hydrodynamic radius $R_{h,app}$ are discussed using dilute water dispersions of homogenous spherical particles poly(N-isopropylacrylamide) microgels, with a simple assumption that the hydrodynamic radius is in proportion to the static radius, when Rayleigh-Gans-Debye approximation is valid. Our results show that the expected values of the normalized time auto-correlation function of the scattered light intensity are consistent with the experimental data very well and the difference between the static radius and the apparent hydrodynamic radius is large and the difference between the hydrodynamic radius and the apparent hydrodynamic radius is influenced by the particle size distribution.

1 Introduction

A great deal of information about particles in dispersion can be obtained using light scattering techniques. One of the main applications of the light scattering techniques is that measure the particle sizes. The static light scattering technique (SLS) obtains the size information from the optical characteristics and the dynamic light scattering technique (DLS) obtains the size information from both the optical and hydrodynamic features of particles.

During the last few decades, the standard method of cumulant is used to obtain the apparent hydrodynamic radius $R_{n,app}$ and its distribution $G(R_{h,app})$ for particles from the normalized time auto-correlation function of the scattered light intensity $g^{(2)}(\tau)$ with the assistance of the Einstein-Stokes relation, where τ is a delay time. The treatment of SLS is simplified to the Zimm plot, Berry plot or Guinier plot etc. to obtain the root mean-square radius of gyration $\langle R_g^2 \rangle^{1/2}$ and the molar mass of particles provided that the particle sizes are

small. In order to obtain more accurate information about the particles, people have explored the relationships between the physical quantities obtained using SLS and DLS techniques. People [[1] − [3]] think that the measurements of the dimensionless shape parameter $\rho = \left\langle R_g^2 \right\rangle^{1/2} / R_{h,app}$ can provide a relatively unambiguous test for the particle shape. In this judgement, there have an assumption that the sizes obtained from SLS and DLS are the same. However, the sizes obtained from SLS and DLS are different physical quantities [[4], [5]]. Exactly using the light scattering techniques, three different sizes can be obtained for homogenous spherical particles: one is static radii R_s obtained from the optical characteristics; the second is hydrodynamic radii R_h obtained from the hydrodynamic features and the third is apparent hydrodynamic radii $R_{h,app}$ determined by the both optical and hydrodynamic characteristics of particles.

In this article, the three different sizes will be discussed using PNIPAM microgel samples with a simple assumption that hydrodynamic radius R_h is in proportion to the static radius R_s. With this simple assumption, the relationship between the SLS and DLS can be built for homogenous spherical particles. Our results show that the expected values of the normalized time auto-correlation function of the scattered light intensity are consistent with the experimental data very well and the difference between the static radius and the apparent hydrodynamic radius is large and the difference between the hydrodynamic radius and the apparent hydrodynamic radius is influenced by the particle size distribution.

2 Theory

For homogeneous spherical particles where the Rayleigh-Gans-Debye (RGD) approximation is valid, the normalized time auto-correlation function of the electric field of the scattered light $g^{(1)}(\tau)$ is given by

$$g^{(1)}(\tau) = \frac{\int_0^\infty R_s^6 P(q, R_s) G(R_s) \exp\left(-q^2 D\tau\right) dR_s}{\int_0^\infty R_s^6 P(q, R_s) G(R_s) dR_s}, \tag{1}$$

where q is the scattering vector, R_s is the static radius, τ is the delay time, D is the diffusion coefficient, $G(R_s)$ is the number distribution and the form factor $P(q, R_s)$ is

$$P(q, R_s) = \frac{9}{q^6 R_s^6} \left(\sin(qR_s) - qR_s \cos(qR_s)\right)^2. \tag{2}$$

In this discussion, the number distribution is chosen as a Gaussian distribution

$$G(R_s; \langle R_s \rangle, \sigma) = \frac{1}{\sigma\sqrt{2\pi}} \exp\left(-\frac{1}{2}\left(\frac{R_s - \langle R_s \rangle}{\sigma}\right)^2\right),$$

where $\langle R_s \rangle$ is the mean static radius and σ is the standard deviation relative to the mean static radius.

From the Stokes-Einstein relation

$$D = \frac{k_B T}{6\pi\eta_0 R_h}, \tag{3}$$

where η_0, k_B, T and R_h are the viscosity of the solvent, Boltzmann's constant, absolute temperature and hydrodynamic radius of a particle, the hydrodynamic radius can be obtained.

For simplicity, we assume that the relationship between the static and hydrodynamic radii can be written as

$$R_h = aR_s, \tag{4}$$

where a is a constant. With the function between the normalized time auto-correlation function of the scattered light intensity $g^{(2)}(\tau)$ and the normalized time auto-correlation function of the electric field of the scattered light $g^{(1)}(\tau)$ [6]

$$g^{(2)}(\tau) = 1 + \beta\left(g^{(1)}\right)^2, \tag{5}$$

the relationship between the static and dynamic light scattering is built and the values of the normalized time auto-correlation function of the scattered light intensity $g^{(2)}(\tau)$ can be expected using the size information obtained from SLS.

If the first cumulant is used to obtain the apparent hydrodynamic radius $R_{h,app}$, the constant a can be determined approximately using

$$a = \frac{R_{h,app}\int_0^\infty R_s^6 P(q,R_s)\,G(R_s)\,dR_s}{\int_0^\infty R_s^7 P(q,R_s)\,G(R_s)\,dR_s}. \tag{6}$$

3 Experiment

The SLS and DLS spectroscopies were measured using the instrument built by ALV-Laser Vertriebsgesellschaft m.b.H (Langen, Germany). It utilizes an ALV-5000 Multiple Tau Digital Correlator and a JDS Uniphase 1145P He-Ne laser to provide a 23 mW vertically polarized laser at wavelength of 632.8 nm.

In this experiment, N-isopropylacrylamide (NIPAM, monomer) from Acros Organics was recrystallized from hexane/acetone solution. Potassium persulfate (KPS, initiator) and N, N'-methylenebisacrylamide (BIS, cross-linker) from Aldrich were used as received. Fresh de-ionized water from a Milli-Q Plus water purification system (Millipore, Bedford, with a 0.2 μm filter) was used throughout the whole experiment. The synthesis of gel particles was described elsewhere [[7], [8]] and the recipes of the batches used in this work are listed in Table 1.

Sample	$T\,(^oC)$	$t\,(hrs)$	$W_N + W_B\,(g)$	$KPS\,(mg)$	n_B/n_N
$PNIPAM-0$	70 ± 1	4.0	1.00	40	0
$PNIPAM-1$	70 ± 1	4.0	1.00	40	1.0%
$PNIPAM-2$	70 ± 1	4.0	1.00	40	2.0%
$PNIPAM-5$	70 ± 1	4.0	1.00	40	5.0%

Table 1. Synthesis conditions for PNIPAM particles.

The four samples were named according to the molar ratios n_B/n_N of N,N'-methylenebisacrylamide over N-isopropylacrylamide. They were centrifuged at 14,500 RPM followed by decantation of the supernatants and re-dispersion in fresh de-ionized water four times to remove of free ions and any possible linear chains. Then the samples were diluted for light scattering to weight factors of 5.9×10^{-6}, 8.56×10^{-6}, 9.99×10^{-6} and 8.38×10^{-6} for $PNIPAM-0$, $PNIPAM-1$, $PNIPAM-2$ and $PNIPAM-5$ respectively. Before the measurements were made, 0.45 μm filters (Millipore, Bedford) were used to do dust free for the samples $PNIPAM-1$, $PNIPAM-2$ and $PNIPAM-5$. Measurements of the normalized time auto-correlation function of the scattered light intensity $g^{(2)}(\tau)$ were performed five times at each angle for all samples except the $PNIPAM-0$ sample, in which measurements were performed only twice.

4 Data Analysis

The mean static radius $\langle R_s \rangle$ and the standard deviation σ of the PNIPAM microgel samples are obtained from the SLS data [9]. For $PNIPAM-1$, the mean static radius $\langle R_s \rangle$, the standard deviation σ and χ^2 obtained at different temperatures are listed in Table 4.1.

Temperature (^oC)	$\langle R_s \rangle (nm)$	$\sigma(nm)$	χ^2
25	277.7±0.5	23.1±0.9	1.84
27	267.1±0.5	23.1±0.8	2.50
29	254.3±0.1	21.5±0.3	2.15
31	224.8±0.9	30.6±0.9	3.31
33	119.9±0.9	19.8±0.6	3.16
36	110.4±0.9	17.3±0.7	4.19
40	111.7±0.9	14.8±0.8	2.73

Table 4.1 The fit results obtained from SLS for $PNIPAM-1$ at different temperatures.

The values of the apparent hydrodynamic radius at different scattering angles were obtained using the first cumulant analysis $[[10]-[12]]$. In order to avoid the consideration for the large values of χ^2, all the fit results obtained using the first cumulant analysis are chosen under this condition $\chi^2 \leqslant 2$. For $PNIPAM-1$ at a temperature of 27^oC, the values of the apparent dynamic radius at different scattering angles are list in Table 4.2. The ratios of the hydrodynamic radius over the static radius calculated using Eq. 6 at different scattering angles also are listed in Table 4.2.

Scattering Angle ($Degree$)	$R_{h,app}\,(nm)$	a
30	329.±4.	1.19
35	331.1±0.7	1.21
40	329.6±0.9	1.21
45	329.8±0.5	1.22
50	329.±1.	1.22
55	326.4±0.2	1.23
60	327.±2.	1.25
65	323.±2.	1.26

Table 4.2 The values of apparent hydrodynamic radius and constant a for $PNIPAM-1$ at different scattering angles and a temperature of 27^oC.

From the results shown in Table 4.2, the value of a almost is a constant. If the value of constant a was set to 1.21, the expected values of $g^{(2)}(\tau)$ calculated using the mean static radius $\langle R_s \rangle$, the standard deviation σ and Eqs. 1 and 5 were compared with the experimental data measured at scattering angles 30^o, 45^o and 60^o, respectively. The results are shown in Fig. 4.1. The results show that the expected values are consistent with the experimental data very well. With the constant a: 1.21, the mean hydrodynamic radius $323.2 \pm 0.6\ nm$ can be obtained and this value only has a little difference with the values of the apparent hydrodynamic radii obtained using the first cumulant at different scattering angles.

From the results shown in Table 4.1, at a temperature of 33^oC, the particle size distribution of the $PNIPAM-1$ sample is wide. The values of the apparent hydrodynamic radius are listed in Table 4.3. The ratios of the hydrodynamic radius over the static radius calculated using Eq. 6 also are listed in Table 4.3. The value of a still almost is a constant. If the value of constant a was set to 1.55, the expected values of $g^{(2)}(\tau)$ calculated using the mean static radius $\langle R_s \rangle$, the standard deviation σ and Eqs. 1 and 5 were compared with the experimental data measured at scattering angles 30^o, 60^o and 90^o, respectively. The results are shown in Fig. 4.2. The results show that the expected values are consistent with the experimental data very well. With the constant a: 1.55, the mean hydrodynamic radius $186. \pm 1.\ nm$ was obtained and the difference between the mean hydrodynamic radius and the apparent hydrodynamic radius is large.

Scattering Angle ($Degree$)	$R_{h,app}\,(nm)$	a
30	212.1±0.6	1.55
35	208.3±0.2	1.53
40	208.7±0.6	1.54
45	207.3±0.3	1.53
50	206.7±0.4	1.53
55	206.±1.	1.53
60	205.±1.	1.53
65	204.9±0.6	1.54
70	205.±1.	1.55
75	205.±1.	1.56
80	205.±1.	1.56
85	205.±1.	1.57
90	203.2±0.7	1.57
95	204.±1.	1.58

Table 4.3 The values of apparent hydrodynamic radius and constant a for $PNIPAM-1$ at different scattering angles and a temperature of 33^oC.

5 Results and Discussion

From the above analysis, three different sizes can be obtained using the light scattering techniques. In general, the values of constant a vary little during the small scattering angle range and the values of the apparent hydrodynamic radius $R_{h,app}$ are a function of the scattering angle. In order to compare the three different sizes conveniently, all the mean hydrodynamic and the apparent hydrodynamic radii were obtained at a scattering angle of 30^o. All three sizes obtained at different temperatures for $PNIPAM-1$ are shown in Fig. 5.1. The picture shows that the difference between the mean static radii and the apparent hydrodynamic radii is large and the difference between the mean hydrodynamic radii and the apparent hydrodynamic radii is influenced by the particle size distribution.

The three different sizes represent the different characteristics of particles. When temperature change from 25^oC to 40^oC, the characteristics of PNIPAM microgel samples change from being hydrophilic to hydrophobic. It is possible that this change makes the different effects on the optical and hydrodynamic characteristics of particles. In order to show the results of this effects, the ratios $R^T_{h,app}/\langle R^T_s\rangle$ and $\langle R^T_h\rangle/\langle R^T_s\rangle$ as a function of temperature T are shown in Figs. 5.2.a and 5.2.b, respectively.

From the fit results for the four PNIPAM microgel sample, the particle size distributions are narrow both below and above the phase transition and are wide near the phase transition. Figure 5.2 shows clearly that the difference between the apparent hydrodynamic radii and the mean hydrodynamic radii is influenced by the distribution widths. For small poly-dispersities, the value of apparent hydrodynamic radius is almost the same as that of the mean hydrodynamic radius. For wide distributions, the part of apparent hydrodynamic radius rep-

resents the effects of the particle size distribution. From the theoretical analysis of cumulant, the apparent hydrodynamic radius is obtained from the average of the term $\exp\left(-q^2 D\tau\right)$ in distribution $G\left(R_s\right)$ with the weight $R_s^6 P\left(q, R_s\right)$, where $\exp\left(-q^2 D\tau\right)$ represents the hydrodynamic features of particles. For the mono-disperse particle systems, since the effects of scattered intensity are cancelled, the apparent hydrodynamic radius is equal to the hydrodynamic radius. For polydisperse particle systems, the apparent hydrodynamic radius shows the total effects of the optical and hydrodynamic characteristics of particles.

Since the PNIPAM microgels possess the temperature sensitivity during the temperature range $15^oC - 50^oC$, a few authors [[13], [14]]used the equilibrium swelling ratios $R_{h,app}^T / R_{h,app}^{T_0}$ to show the volume phase transition. For our samples, the volume phase transition during the temperature range $25^oC - 40^oC$ is shown in Fig. 5.3 using the equilibrium swelling ratios of the mean static radii and the apparent hydrodynamic radii, respectively. All radii are compared to that measured at a temperature of 40^oC. The ratios of $\left\langle R_s^T \right\rangle / \left\langle R_s^{40^oC} \right\rangle$ and $R_{h,app}^T / R_{h,app}^{40^oC}$ are shown in Fig. 5.3.a and b respectively.

From the chemical knowledge, the materials of PNIPAM possess the temperature sensitivity. If adding the N, N'-methylenebisacrylamide, the temperature sensitivity of PNIPAM microgels will be influenced by the content of the N, N'-methylenebisacrylamide which does not possess the temperature sensitivity. If the content of the N, N'-methylenebisacrylamide continues to increase, the temperature sensitivity of PNIPAM microgels is becoming weak. Figure 5.3 clearly shows the feature. The phase transition of PNIPAM microgels, indicated as the ratios $\left\langle R_s^T \right\rangle / \left\langle R_s^{40^oC} \right\rangle$ or $R_{h,app}^T / R_{h,app}^{40^oC}$ as a function of T, becomes less sharp and occurs in a broader T range as the N, N'-methylenebisacrylamide content is increased.

6 Conclusion

The average scattered intensity is determined by the optical characteristics of particles in dispersion. The normalized time auto-correlation function of the scattered light intensity $g^{(2)}\left(\tau\right)$ includes both the optical and hydrodynamic information of particles. Using the light scattering techniques, three different particle sizes can be measured. The static radius represents the optical characteristics, the hydrodynamic radius shows the hydrodynamic features and the apparent hydrodynamic radius represents both the optical and hydrodynamic characteristics of particles. For narrow distributions, the value of the apparent hydrodynamic radius is a good approximation of the mean hydrodynamic radius. In general, the sizes obtained from SLS and DLS are different. If the relationship between the optical and hydrodynamic features of particles can be understood, the accurate relationship between the SLS and DLS can be built. Then the static sizes also can be obtained from the DLS data. The accurate relationship between the optical and hydrodynamic features of particles can be further explored.

Fig. 4.1 The expected and experimental values of the normalized time auto-

correlation function of the scattered light intensity $g^{(2)}(\tau)$ for $PNIPAM-1$ at a temperature of 27^oC. The symbols show the experimental results and the line shows the calculated values with the simple assumption $R_h = 1.21R_s$.

Fig. 4.2 The expected and experimental values of the normalized time autocorrelation function of the scattered light intensity $g^{(2)}(\tau)$ for $PNIPAM-1$ at a temperature of 33^oC. The symbols show the experimental results and the line shows the calculated values with the simple assumption $R_h = 1.55R_s$.

Fig. 5.1 Values of the apparent hydrodynamic radii (⧫) , the mean hydrodynamic radii (▲) at a scattering angle of 30^o and the mean static radii (•) for $PNIPAM-1$ at different temperatures.

Fig. 5.2 The comparisons for three different sizes obtained using light scattering technique. a). The ratios $R^T_{h,app}/\left\langle R^T_s\right\rangle$ of the apparent hydrodynamic over the mean static radii are shown. b). The ratios $\left\langle R^T_h\right\rangle/\left\langle R^T_s\right\rangle$ of the mean hydrodynamic over the mean static radii are shown for $PNIPAM-0$, $PNIPAM-1$, $PNIPAM-2$ and $PNIPAM-5$ during the temperature range from 25^oC to 40^oC.

Fig. 5.3 The volume phase transition of $PNIPAM-0$, $PNIPAM-1$, $PNIPAM-2$ and $PNIPAM-5$. a). The phase transition was shown using the ratios of the mean static radii $\left\langle R^T_s\right\rangle$ at temperature T to that $\left\langle R^{40^oC}_s\right\rangle$ at 40^oC. b). The phase transition was shown using the ratios of the apparent hydrodynamic radii $R^T_{h,app}$ at temperature T to that $R^{40^oC}_{h,app}$ at 40^oC.

References

[1] S. U. Egelhaaf and P. Schurtenberger. J. Phys. Chem., 1994, 98, 8560.

[2] W. Burchard, K. Kajiwara and D. Nerger. J. Polym. Sci., 1982, 20, 157.

[3] W. Burchard, M. Schmidt and W. H. Stockmayer. Macromolecules, 1980, 13, 1265.

[4] Y. Sun. Unpublished (Please see my first paper).

[5] Y. Sun Unpublished (Please see my third paper).

[6] P. N. Pusey in Neutrons, X-rays and Light: Scattering Methods Applied to Soft Condensed Matter, edited by P. Lindner and Th. Zemb, Elsevier Science B.V., Amsterdam, The Netherlands, 2002.

[7] J. Gao and B. J. Frisken, Langmuir, 2003, 19, 5217

[8] J. Gao and B. J. Frisken, Langmuir, 2003, 19, 5212

[9] Y. Sun Unpublished (Please see my second paper)

[10] B. J. Berne and R. Pecora. Dynamic Light Scattering. Robert E. Krieger Publishing Company, Malabar, Florida, 1990.

[11] D. E. Koppel. J. Chem. Phys., 1972, 57, 4814.

[12] J. C. Brown, P. N. Pusey and R. Dietz. J. Chem.Phys., 1975, 62, 1136.

[13] X. Zhang, D. Wu and C. Chu. J. Polym. Sci.: Part B: Polymer Physics, 2003, 41, 582.

[14] K. Kratz and W. Eimer. Ber. Bunsenges. Phys. Chem. 1998, 102, 848.

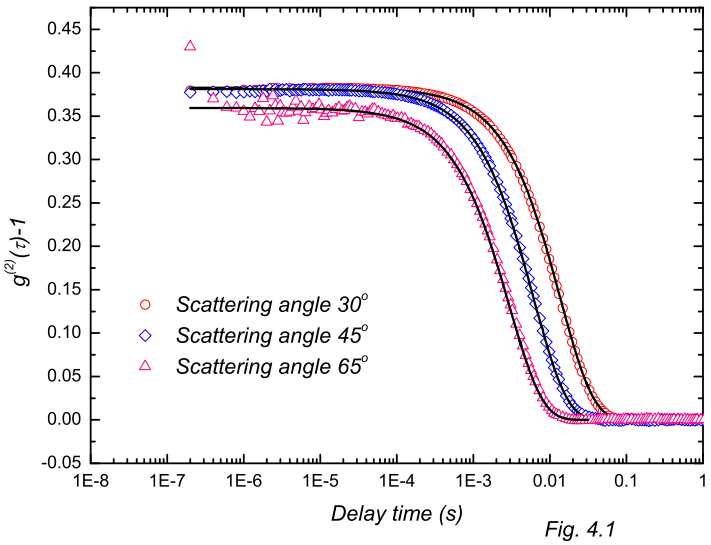
0.45
0.40
0.35
0.30
0.25
0.20
0.15
0.10
0.05
0.00
-0.05
$g^{(2)}(\tau)$-1
1E-8
1E-7
1E-6
1E-5
1E-4
1E-3
0.01
0.1
1
Delay time (s)
Scattering angle 30°
Scattering angle 45°
Scattering angle 65°

Fig. 4.1

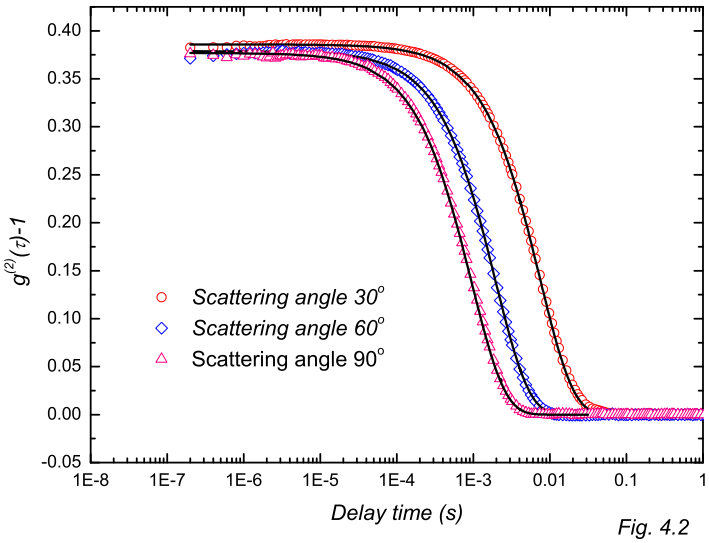
0.40
0.35
0.30
0.25
0.20
0.15
0.10
0.05
0.00
-0.05
$g^{(2)}(\tau)$-1
1E-8
1E-7
1E-6
1E-5
1E-4
1E-3
0.01
0.1
1
Delay time (s)
Scattering angle 30°
Scattering angle 60°
Scattering angle 90°

Fig. 4.2

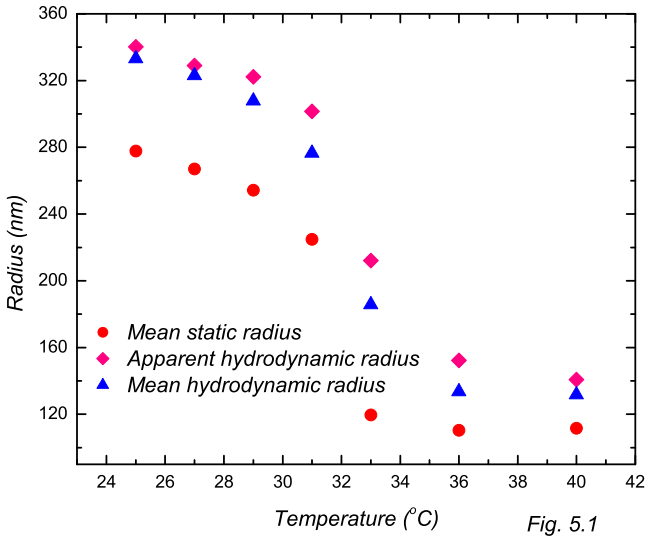
360
320
280
240
200
160
120
Radius (nm)
24
26
28
30
32
34
36
38
40
42
Temperature (°C)
Mean static radius
Apparent hydrodynamic radius
Mean hydrodynamic radius

Fig. 5.1

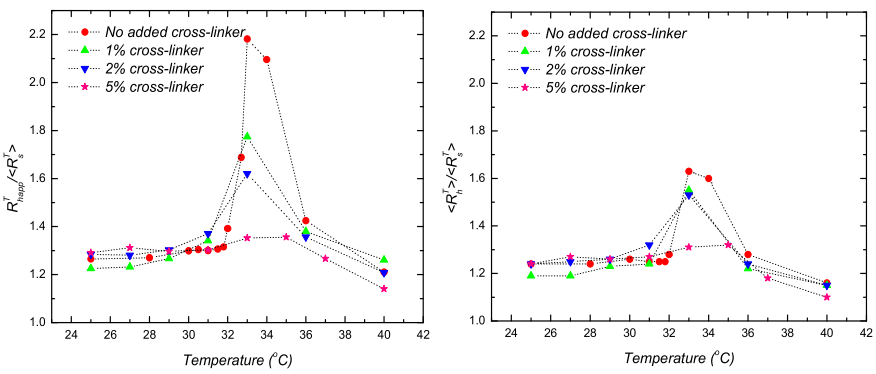
No added cross-linker
1% cross-linker
2% cross-linker
5% cross-linker
$R^T_{happ}/<R^T_s>$
Temperature (°C)
No added cross-linker
1% cross-linker
2% cross-linker
5% cross-linker
$<R^T_h>/<R^T_s>$
Temperature (°C)

Fig. 5.2

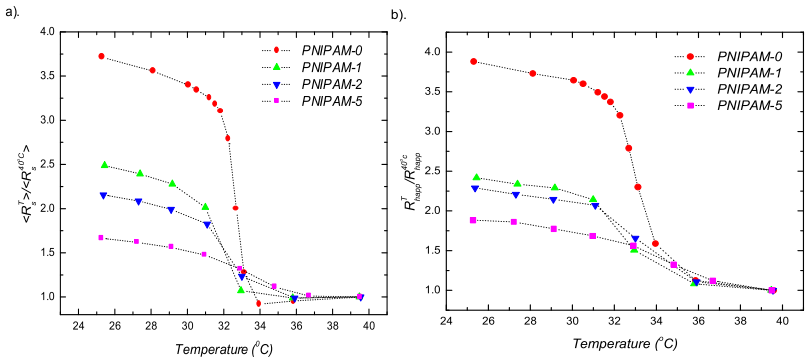
a).
b).
PNIPAM-0
PNIPAM-1
PNIPAM-2
PNIPAM-5
Temperature (°C)
Temperature (°C)

Fig. 5.3